

Near-wall Coherent Structure Generation in a Turbulent Boundary Layer

Wade Schoppa and Fazle Hussain

Department of Mechanical Engineering
University of Houston, Houston, TX 77204-4006 USA

Abstract

We present new insight into the generation of streamwise vortices near the wall, and an associated drag reduction strategy. Growth of x -dependent spanwise velocity disturbances $w(x)$ is shown to occur via two mechanisms: (i) linear transient growth, which dominates early-time evolution, and (ii) linear normal-mode instability, dominant asymptotically at late time (for frozen base flow streaks). Approximately 25% of streaks extracted from near-wall turbulence are shown to be strong enough for linear instability (above a critical vortex line lift angle). However, due to viscous cross-diffusion of streak normal vorticity ω_y , normal mode growth ceases after a factor of two energy growth. In contrast, the linear transient disturbance produces a 20-fold amplification, due to its rapid, early-time growth before significant viscous streak decay. Thus, linear transient growth of $w(x)$ is revealed as a new, apparently dominant, generation mechanism of x -dependent turbulent energy near the wall. Combined transient growth/instability of lifted, vortex-free low-speed streaks (above the instability cutoff of streak strength) is shown to generate new streamwise vortices, which dominate near-wall turbulence phenomena. Significantly, the 3D features of the (instantaneous) vortices generated by transient/instability growth agree well with the coherent structures deduced (*i.e.* ensemble-averaged) from fully turbulent flow, suggesting the prevalence of this mechanism. Results suggest promising new strategies for drag and heat transfer control, involving large-scale (hence more durable) actuators, without requiring wall sensors or control logic.

1. Introduction

There is an evolving consensus that the increased drag and heat transfer in turbulent boundary layers are due to near-wall vortical *coherent structures* (CS). Viable control of near-wall turbulence, as yet largely unrealized in practice, has the potential for enormous savings in fuel costs via drag reduction for aircraft, marine transport vehicles, pipelines, and heat transfer management for high-temperature gas turbines. Although a barrage of drag reduction strategies have been studied extensively, their engineering application has remained scarce. A lack of successful implementation of boundary layer control can generally be traced to two key difficulties: (i) tiny spatial scales of near-wall streamwise CS (~ 0.1 mm) and (ii) incomplete understanding of the dynamics of CS initiation and evolution.

To address these inherent obstacles, we propose here new control approaches which explicitly utilize recent advances in the understanding of near-wall turbulence physics. The prominence of streamwise vortical coherent structures (CS) in near-wall turbulence is now well accepted (*e.g.* see [11]), as is their critical role in the elevated drag in turbulent boundary layers. The transport enhancing effect of near-wall CS is well understood. These CS sweep near-wall fluid toward the wall on one CS flank and eject it away from the wall on the other. Drag and heat transfer are

enhanced by the wallward motion, which steepens the wall gradients of streamwise velocity U . Note that the gradient reduction on the outward motion side of vortices is relatively smaller, resulting in enhancement of mean wallward momentum transfer due to near-wall vortices.

The most logical approach to CS-based reduction of drag and heat transfer is to simply prevent vortex regeneration in the first place (in contrast to many approaches which counteract the wall interaction of fully developed CS). Although it has long been hypothesized that a major source of turbulence production near the wall is the instability of inflectional low-speed streaks (*e.g.* [2, 10, 16]), the issue remains unresolved. In particular, it is currently unknown whether streaks of sufficient strength for instability actually occur in fully-developed near-wall turbulence. Additionally, the influence on streak instability growth of viscous annihilation of streak normal vorticity is yet to be quantified, as is the possibility of linear transient growth. Finally, the relationship between streak disturbance growth and the formation mechanism of longitudinal vortices is poorly understood, which has prevented the development of streak disturbance control strategies aimed at drag reduction (*e.g.* [3,4]).

To date, we have demonstrated [13] that the CS [5,6] extracted from fully developed near-wall turbulence can be directly created by 3D inviscid instability of lifted streaks near a single wall (created by previous "parent" vortices, no longer present), the generation mechanism being akin to that of streamwise vortices in free shear layers by oblique mode instability [12]. This new-found association of near-wall CS formation with instability mechanisms opens up promising avenues for explaining and especially controlling near-wall turbulence, noting the documented success of experimental instability control in both free- and wall-bounded shear flows (*e.g.* see [3]).

To suppress CS via control of streak disturbance growth (responsible for CS formation), there are two possibilities: either (i) counteract existing perturbations which would otherwise generate new CS, or (ii) stabilize the base flow streaks. Pursuit of (i) would necessitate instantaneous and small-scale detection and control, which would suffer from the durability problems faced by microscale active wall elements. Approach (ii) is very attractive from the standpoint of large-scale (hence more robust) control, wherein numerous (perhaps thousands of) streaks may be stabilized together – hence suppressing new CS formation over an extended spatial domain – with a single robust actuator, involving time-independent control and no flow sensing [15].

The primary objective of this paper is to summarize our latest findings regarding streak disturbance growth, vortex generation, and associated drag reduction strategies. We first demonstrate the underlying mechanism of CS formation, driven by nonlinear evolution of 3D disturbances of lifted low-speed streaks, distinguishing between linear (normal-mode) instability and linear transient growth.

2. Computational Approach

In the following, we address streak instability-induced vortex generation and its control using direct numerical simulations of the Navier-Stokes equations. Periodic boundary conditions are used in x and z , and the no-slip condition is applied on the two walls normal to y ; see Kim *et al.* [9] for the simulation algorithm details. To better isolate instability and the subsequent vortex formation, we use the minimum outer Reynolds number $Re=U_c h/\nu=2000$ (U_c is the centerline velocity of the $2h$ wide channel for a laminar flow with the same volume flowrate) and the minimum domain sizes in x and z for sustained channel flow turbulence – the so-called “minimal flow unit” of Jimenez & Moin [7]. For the simulations of isolated vortex regeneration, a constant volume flux is maintained, and $32 \times 129 \times 32$ grid points are used in x , y , and z respectively. The control simulations are initialized with full-domain channel flow turbulence at $Re=1800$ and 3200 [9], with $48 \times 65 \times 48$ and $192 \times 129 \times 192$ dealiased Fourier modes respectively. Actuation is represented by an applied control flow – either maintained at a constant amplitude or allowed to freely evolve – superimposed onto the turbulence.

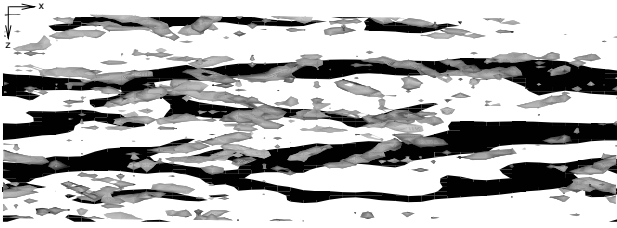


Figure 1. Lifted low-speed streaks (black) illustrated by $u' < 0$ at $y^+ = 20$ and streamwise vortices (grey) indicated by the Jeong & Hussain [5] vortex definition in the region $0 < y^+ < 60$.

3. Disturbance Growth of Near-Wall Streaks

The two most prominent structural features of near-wall turbulence are illustrated in figure 1: (i) “streaks” of low momentum fluid which has been lifted into the buffer region, and (ii) elongated longitudinal vortices, illustrated by the Jeong & Hussain [5] vortex definition. It is now well-accepted that the streaks are generated by the lifting of low-speed fluid near the wall by the normal velocity induced by streamwise vortices; this is consistent with the close proximity of streaks to streamwise vortices in figure 1.

3.1 Linear Instability

To evaluate the role of streak instability in vortex generation, we first consider three-dimensional disturbances of a class of two-dimensional base flows, representing the range of low-speed streak strengths (*i.e.* magnitude of ω_y^+ flanking streak, defined later as θ_{20}) observed in fully-developed near-wall turbulence. To isolate the three-dimensional dynamics of lifted streaks, we analyze a z -periodic row of parallel (x -independent) low-speed streaks, initially containing no vortices or ω_x whatsoever (*i.e.* $U(y,z)$ only). Additionally, the streaks are localized to a single wall, to prevent the second wall (far removed in z) from strongly influencing the essential near-wall dynamics, such influence being minimal in channel and plane Couette flows at sufficiently high Re . Note that this class of base flows is inviscidly steady (for a constant volume

flux) as required for stability analysis, and is qualitatively consistent with near-wall streaks observed both in minimal (*e.g.* see [7,13]) and full-domain (*e.g.* see [11]) turbulent flow.

As a representation of vortex-free, lifted low-speed streaks of variable strength, we consider a base flow family of the form

$$U(y,z) = U_0(y) + (\Delta u/2) \cos(\beta_s z) g(y), \quad (1)$$

$$V = W = 0,$$

where $U_0(y)$ is the turbulent mean velocity profile and $g(y)$ is an amplitude function which satisfies the no-slip condition at $y=0$ and localizes the streaks’ velocity defect to a single near-wall region (*i.e.* $y^+ < 60$). A function satisfying these requirements is $g(y) = y \exp(-\sigma y^2)$, normalized to unity and with σ specified such that the maximum streak vorticity $\omega_{y|_{\max}} = \beta_s \Delta u/2$ and normal circulation per unit length Δu occur in the range $y^+ = 20-30$, consistent with lifted streaks.

As illustrated in figure 2b for a moderately strong streak (circulation specified with Δu in (1)), the base flow (1) closely resembles lifted low speed streaks prominent both in minimal channel turbulence (figure 2a) and in virtually any (y,z) cross-section of full-domain turbulence (*e.g.* see Kim *et al.* 1987). In accordance with (1), all streak base flows considered here are even-symmetric about $z=0$, *i.e.* $U(y,z) = U(y,-z)$.

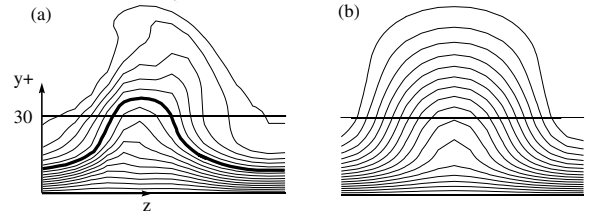


Figure 2. Lifted low-speed streak in near-wall turbulence, illustrated by (a) a typical cross-stream distribution of U , approximated by (b) the analytical base flow (1) used for stability analysis. The bold contour shown in (a) is the $0.55U_c$ contour.

For illustrative purposes, it is useful to represent the “strength” of lifted streaks in terms of the maximum inclination angle θ of vortex lines on the streak flank, given locally by $\theta = \tan^{-1}(|\omega_y|/|\omega_z|)$. In this way, the strength of the base flow streaks (1) may be characterized conveniently as the maximum vortex line lift angle, *e.g.* defined at $y^+ = 20$ as $\theta_{20} = \tan^{-1}[\omega_{y|_{\max}}/(dU_0/dy(y^+ = 20))]$ with $\omega_{y|_{\max}} = \beta_s \Delta u/2$. For all flows considered here, the streak spanwise wavenumber β_s in (1) is chosen as $2\pi/\beta_s^+ = 100$, corresponding to a 100 wall unit spanwise spacing of adjacent low-speed streaks.

In accordance with Floquet theory for the z -periodic base flows represented in (1), we consider temporal disturbances (denoted by primes) of the form

$$\begin{pmatrix} u' \\ v' \\ w' \\ p' \end{pmatrix} (x, y, z, t) = \Re \left[\begin{pmatrix} \tilde{u} \\ \tilde{v} \\ \tilde{w} \\ \tilde{p} \end{pmatrix} (y, z) e^{i(\alpha x + \beta z)} e^{\sigma t} \right], \quad (2)$$

where the streamwise α and spanwise wavenumber β are real, and the eigenvalues σ are generally complex. The tilded complex eigenfunctions are periodic in z with the streak spanwise wavenumber β_s , and the velocity eigenfunctions vanish at the upper and lower walls ($y=0, 2h$).

To quantify possible linear instability of streaks characteristic of fully-developed near-wall turbulence, we first discuss three-dimensional solutions of the stability equations for the class of streaks represented by the base flow (1). Realizable characteristics of streaks in near-wall turbulence are then obtained via a streak eduction procedure, permitting a statistical evaluation of these streaks' degree of instability.

We analyze the instability of the streak flow (1) using direct numerical simulations of the Navier-Stokes equations, initialized with effectively infinitesimal disturbances of the form

$$w(x,y)=\varepsilon \sin(\alpha x)y \exp(-\sigma y^2), \quad (3)$$

where ε is the (linear) disturbance amplitude and σ is a normal decay parameter which localizes the perturbation to the near-wall region ($y^+ < 60$). Provided that an arbitrary perturbation such as (3) has a non-zero projection onto the instability mode of interest, the disturbance will naturally evolve to this eigenmode. Lock-on of the simulation to a given instability mode is signaled by sustained exponential growth of $E_{1n}(t)$ (with $n \neq 0$), the volume-integrated energy in all Fourier modes with an x -wavenumber of α .

As indicated in figure 3, a moderately strong streak with $\omega_{y^+}|_{\max}=0.35$ (streak lift angle $\theta_{20}=56^\circ$) and $2\pi/\beta_s^+=100$ (figure 2b) is indeed linearly unstable, with a maximum growth rate of approximately $\sigma^+=0.012$ (*i.e.* doubling of three-dimensional energy in 29 wall time units). Interestingly, the maximal growth rate occurs for a streamwise wavelength of approximately 300 wall units, closely corresponding to the minimum x -wavelength required for turbulence sustenance [7] at $Re=2000$ ($L_x^+=290$). Note that the 400 wall unit streamwise extent of a symmetric pair of educed near-wall coherent structures [6] also exhibits a nearly maximal streak instability growth rate. Collectively, these results indicate that the characteristic streamwise wavelength of near-wall structures (300-400 wall units) is consistent with a predominant streak instability mechanism [14].

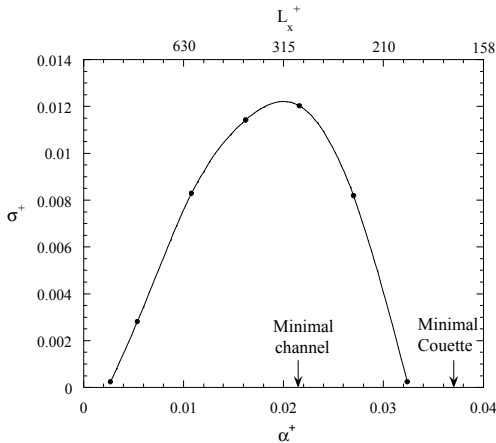


Figure 3. Growth rate of most-unstable sinuous mode versus streamwise wavenumber, for streak distribution in figure 1 with $\omega_{y^+}|_{\max}=0.35$, corresponding to a streak lift angle of $\theta_{20}=56^\circ$.

Having shown linear instability of a $U(y,z)$ distribution visually representative of instantaneous lifted streaks in near-wall turbulence, we now quantify the growth rate variation with streak strength, defined in terms of the lift angle θ_{20} (defined above). Significantly, sinuous streak instability requires a threshold streak lift angle θ_{20} of approximately 50° (corresponding to a streak

vorticity of $\omega_{y^+}|_{\max}=0.27$), reflected by the region of positive growth rate σ in figure 4. Thus, lifted streaks may be either passive (stable) or dynamically active (unstable) to small-amplitude sinuous perturbations, depending upon rather slight (*i.e.* virtually indistinguishable visually) differences in streak vorticity. Past the instability cutoff, the growth rate increases approximately linearly with the streak vorticity $\omega_{y^+}|_{\max}$ (nearly linearly with θ_{20} for this angle range), suggesting a dominant influence of $U(z)$ shear in driving sinuous instability (see also Yu & Liu [18] for Gortler streaks). Nevertheless, as shown below, the sinuous mode is inherently three-dimensional, and its growth mechanism is distinct from that of a one-dimensional $U(z)$ wake profile. Based on the instability cutoff behavior in figure 4 (consistent also with the stability of the turbulent mean profile $U(y)$ for channel flow), the straightening of streak vortex lines by background ω_z is a strongly stabilizing effect for sinuous streak instability.

Owing to the threshold behavior in figure 4, the role of (linear) streak instability in fully developed near-wall turbulence relies critically on the magnitudes of streak $\partial u/\partial z$ (hence streak lift angle) actually realized. To obtain conditional streak statistics, an eduction procedure is used to extract individual streak realizations from fully developed turbulent channel flow at $Re=1800$ (Kim *et al.* [9] database).

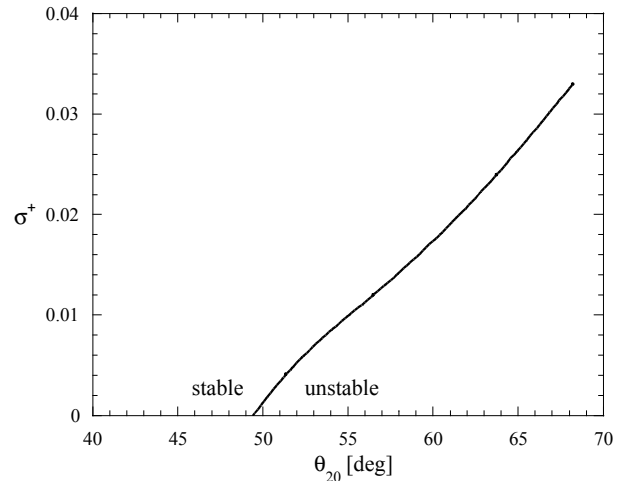


Figure 4. Dependence of sinuous mode growth rate on streak vortex line angle θ_{20} at $Re=2000$, illustrating threshold of streak lifting required for streak instability growth.

The histogram of streak lift angle statistics for fully-developed near-wall turbulence are shown in figure 5 at eduction locations of $y^+=20$. Analogous to the definition of θ_{20} above, the streak lift angle at a general y is defined as $\theta_n = \tan^{-1} [|\partial u/\partial z|_{\max} / (dU_0/dy)]_{y^+=n}$. At $y^+=20$, comparison of lift angle statistics (figure 5) with the corresponding streak instability growth rate (figure 4) indicates that approximately 25% of near-wall streaks are strong enough (*i.e.* with sufficient $\partial u/\partial z$) to be linearly unstable. At $y^+=10$ and $y^+=30$ as well, streaks stronger than the neutrally stable analytical streak (of the form (1)) occur in fully-developed turbulence. (Thus, not all streaks detected in the buffer layer are strong enough to become unstable.)

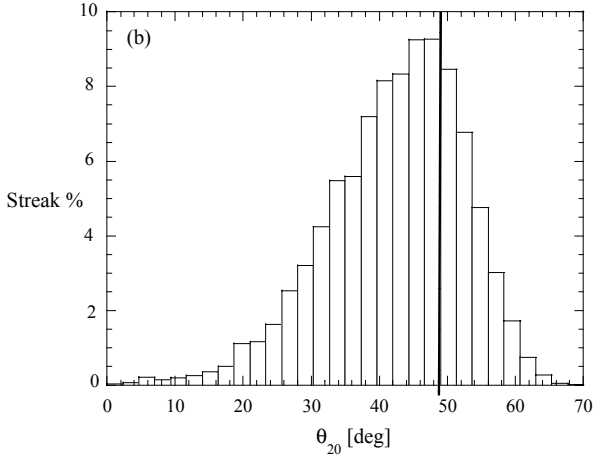


Figure 5. Histogram of conditional streak vorticity statistics, for streaks educed at $y^+=20$, from fully developed channel flow turbulence. The bold line denotes the instability cutoff in figure 4.

In summary, streaks of sufficient strength for linear instability are in fact realized in the buffer layer. In contrast, most streaks nearer to the wall are numerous, but do not have sufficient lift angles to be linearly unstable and hence are dynamically passive with respect to streak instability. Hence, a scenario of predominant vortex generation and turbulence sustenance via linear instability of lifted near-wall streaks must be evaluated carefully, as undertaken below.

3.2 Linear Transient Growth

We now consider the linear evolution of the instability eigenmode and other x -dependent disturbances of unfrozen, viscously decaying streaks. As shown in figure 6 for an initially unstable streak with $\theta_{20}=56^\circ$, the normal mode growth is arrested at $t^+\sim 50$ by the streak diffusion, resulting in a factor of two 3D energy growth (i.e. all x -dependent modes). Note that the typical nonlinear (finite amplitude) saturation is not occurring here. Instead, attenuation is due primarily to cross-diffusion (i.e. viscous annihilation, a kind of planar reconnection) of the opposite-signed ω_y flanking the low-speed streak. In fact, ω_y is reduced to 70% of its initial value by the E_{3D} saturation time, indicating that the (exponential) streak decay rate due to cross-diffusion is non-negligible (approximately half the instability growth rate).

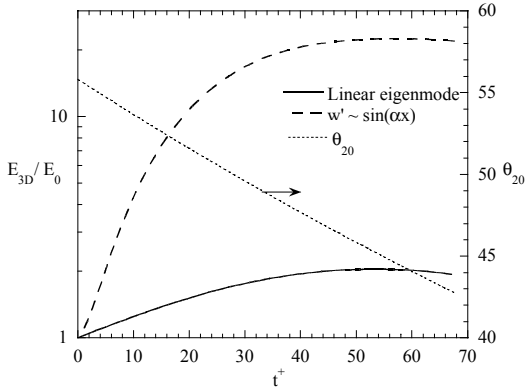


Figure 6. Evolution of 3D energy (all x -dependent modes), for most unstable linear eigenmode (solid) and $w(x)$ linear transient disturbance (dashed). The viscous streak annihilation is reflected by the decreasing streak vortex line lift angle (dotted).

Significantly, much more significant growth of the arbitrary $w(x)$ perturbation (3) occurs for the same base flow streaks, producing a factor of 20 energy growth (figure 6). Recalling the modest factor of two growth of the normal eigenmode, the dominant growth of the $w(x)$ disturbance (3) indicates that its initial rapid amplification is due to *linear transient growth* (see Trefethen *et al.* [17] for a review of the transient growth concept). In short, transient growth of disturbances is possible for non self-adjoint (i.e. non-normal) linearized Navier-Stokes operators, such as derived here for disturbances of two-dimensional streaks. Recall that eigenmodes of traditional normal mode stability problems are not orthogonal to one another if the corresponding linear operator is non-normal. In this case, particular disturbances (including specific combinations of normal eigenmodes) can generally be amplified by significant factors (i.e. linear transient growth), even if all normal eigenmodes are individually stable.

In figure 6, the early-time evolution of the disturbance (3) is dominated by non-normal mode transient growth (the only means for disturbance growth to exceed that of the most unstable normal mode). Note that the disturbance (3) eventually locks-on to the normal mode and hence excites both the non-normal transient disturbance and the normal eigenmode. Further, the relevance of the disturbance (3) in the actual flow is supported by observations of x -alternating quadrant 2 and 3 uw Reynolds stress events in near-wall turbulence. As further clear evidence of non-normal transient growth, the $w(x)$ disturbance (3) produces a factor of 7 energy growth for linearly stable streaks (i.e. no growth due to stable normal eigenmode), growth which is maintained into the nonlinear regime (figure 7). Finally, note the distinction of the linear transient growth of streaks $U(y,z)$ revealed here, with the linear transients of the mean profile $U(y)$ studied extensively to date (see e.g. [1]).

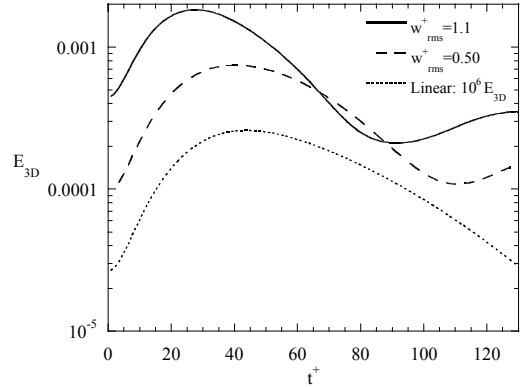


Figure 7. Evolution of 3D energy for $w(x)$ transient disturbance of a linearly stable streak with $\theta_{20}=45^\circ$, for both linear (dotted) and finite-amplitude initial disturbance amplitudes.

4. Nonlinear evolution and vortex formation

Having confirmed that (one-walled) streaks with sufficient y circulation can experience significant growth of x -dependent disturbances via a combined linear transient/instability mechanism, we now consider the subsequent nonlinear evolution using DNS. Results clearly illustrate the genesis of streamwise CS, near-wall shear layers, and arch vortices, suggesting that streak disturbance growth is the dominant mechanism of vortex generation and thus turbulence production. Most significantly, as the mode grows to a nonlinear amplitude (initially $w^+/U_c = 1\%$ at $y^+=30$), new collapsed

streamwise vortices are directly created (figure 8a-c). At early times, disturbance growth is characterized by increased circulation of flattened ω_x sheets, with the spanwise symmetry of the linear eigenmode approximately maintained. Subsequently, as nonlinear effects (described below) become prominent, $+\omega_x$ begins to concentrate on the $+z$ flank of the low-speed streak (figure 8b). By symmetry, the ω_x distribution at a half wavelength in x away is obtained by z reflection and sign inversion; thus, $-\omega_x$ is generated on the $-z$ flank here. As this ω_x amplification continues, collapsed (*i.e.* with compact cross-section) streamwise vortices quickly emerge (figure 8c). This genesis of new vortices from ω_x layers is strikingly similar to that frequently observed in minimal channel flow.

Previous studies (*e.g.* Jimenez & Orlandi [8]) have focused on wall vorticity layer rollup due to (2D) self-advection (and image vorticity due to wall impenetrability). In the streak disturbance evolution described here, the vortex formation is not in reality a rollup process; the formation is inherently 3D, dominated by intense ω_x stretching. Even well past their initial formation, streamwise vortices and hence turbulence continue to be sustained (*e.g.* figure 8d), indicating the importance of this streak disturbance mechanism to turbulence sustenance.

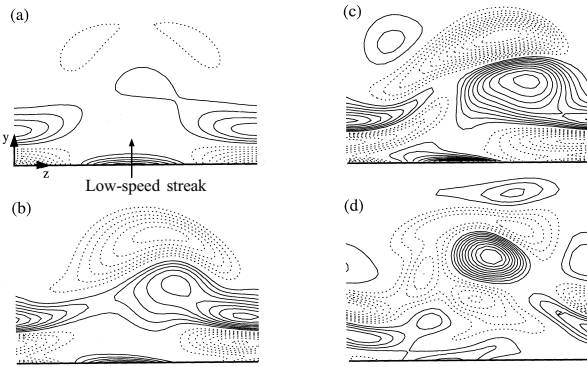


Figure 8. Streamwise vortex formation due to finite-amplitude streak instability, illustrated by cross-stream distributions of ω_x at (a) $t^+=17$, (b) $t^+=51$, (c) $t^+=103$, (d) $t^+=928$. Planes in (b) and (c) are tracked with the instability phase speed of approximately $0.6U_c$.

The 3D geometry of the newly generated vortices (figures 9a,b) (say, the x -overlapping of tilted, opposite-signed streamwise vortices on either side of a low-speed streak) agrees well with the typical flow structure during the active phase of minimal channel regeneration. Most significantly, this vortex geometry (maintained upon evolution except for increasing overlap) is strikingly similar to that of 3D CS educed (from more than 100 vortex realizations) in full-domain turbulence (figure 10), which has been shown to capture all important near-wall events [6]. Irregularities (*e.g.* kinks) of the base flow streaks and finite-amplitude incoherent turbulence will surely occur, causing variations in vortices from one realization to another. If an underlying instability mechanism is present, it should be revealed by ensemble averaging over a large number of base flow/perturbation combinations, *i.e.* by CS education. The close correspondence of figures 9 and 10 indicates that this is in fact the case, serving as strong evidence that this vortex formation process is a dominant mechanism in near-wall turbulence.

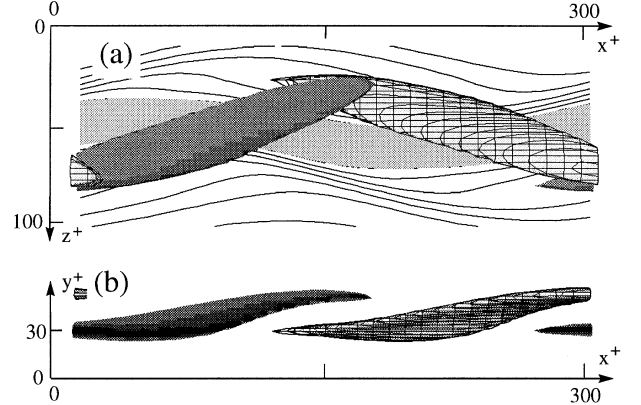


Figure 9. Streamwise vortices' (x,z) plane tilting, x -overlapping, and location relative to a low-speed streak in (a) top view, (b) side view. The 80% isosurfaces of $+\omega_x$ and $-\omega_x$ at $t^+=103$ are (dark) shaded and hatched respectively; contours of u at $y^+=20$ are overlaid in (a), with low levels of u light-shaded to demarcate the low-speed streak.

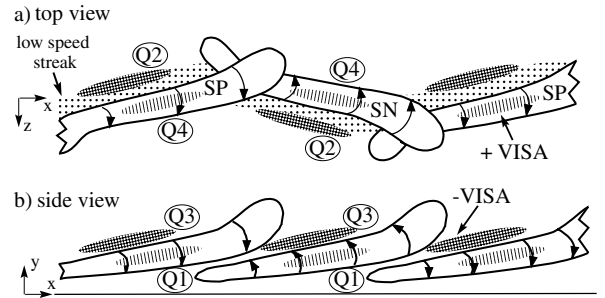


Figure 10. Near-wall educed CS and associated coherent events (adapted from Jeong *et al.* [6]); including \pm VISA events ($\pm\partial u/\partial x$); quadrant Re stresses Q1, Q2 (ejection), Q3, and Q4 (sweep); and a kinked low-speed streak.

Since the newly generated vortices are predominantly streamwise (figure 9a), the essential dynamics of vortex formation are those of ω_x , whose inviscid evolution is governed by

$$\frac{\partial \omega_x}{\partial t} = -u \frac{\partial \omega_x}{\partial x} - \underbrace{v \frac{\partial \omega_x}{\partial y} - w \frac{\partial \omega_x}{\partial z}}_{\text{Advection}} + \underbrace{\omega_x \frac{\partial u}{\partial x}}_{\text{Stretching}} + \underbrace{\frac{\partial v}{\partial x} \frac{\partial u}{\partial z} - \frac{\partial w}{\partial x} \frac{\partial u}{\partial y}}_{\text{Tilting}} \quad (4)$$

In figure 11, we observe that the circulation of the elongated near-wall ω_x layers (figure 11a) increases due to vortex line tilting, given by the latter production term $-(\partial w/\partial x)(\partial u/\partial y)$ (figure 11c), which dominates the former. Although typically largest in magnitude over all other, the $-(\partial w/\partial x)(\partial u/\partial y)$ term actually generates a flattened tail in the near-wall ω_x layer (C in figure 7c), *not* a vortex. Contrary to prior speculation, these layers do not roll up due to their self-advection – a purely 2D mechanism. In fact, the cross-stream

transport (B in figure 11b) actually opposes the rollup process, due to the opposite-signed ω_x immediately overhead (SN in figure 11a). In reality, vortex formation is due to direct stretching of $+\omega_x$ on the $+z$ flank of the low-speed streak (also, $-\omega_x$ amplification on the $-z$ flank, at a half x wavelength away), evident from nearly circular regions of $+\omega_x \partial u / \partial x$ there (D in figure 11d). We find that this local ω_x stretching is sustained in time and is mainly responsible for the vortex collapse, whose location coincides with the $+\omega_x \partial u / \partial x$ peak. In turn, the positive $\partial u / \partial x$ responsible for vortex collapse by stretching is a simple consequence of low-speed streak waviness, illustrated in figure 9(a). Recall that streak waviness is generated both by (linear) transient growth and sinuous streak instability. Once this waviness grows to a finite size, strong $+\partial u / \partial x$ develops downstream of the streak crests, causing direct stretching of positive (SP) and negative (SN) ω_x existing there. Since a large velocity difference exists across the streak flanks (with vorticity comparable to the mean velocity gradient at the wall), a sizable value of $+\partial u / \partial x$ is quickly generated by the rapidly growing streak wave. The initial ω_x sheets (figure 8a) then suddenly collapse (figure 8c) due to localized stretching (figure 11d), overcoming viscous diffusion which would otherwise cause their annihilation (on a similar timescale as the collapse). Note that these dynamics are also captured as (ensemble-averaged) +VISA events (*i.e.* $+\partial u / \partial x$) existing within the CS core (figure 10), indicating that this vortex generation process is indeed a dominant one.

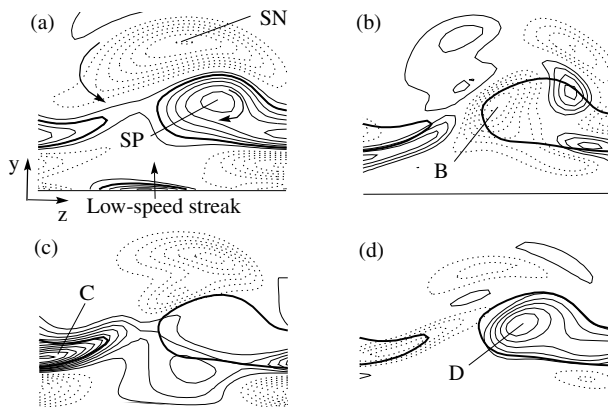


Figure 11. Distributions of (a) ω_x , and selected terms of the ω_x evolution equation: (b) self-induction (cross-stream), (c) the $-(\partial w / \partial x)(\partial u / \partial y)$ tilting term, and (d) direct stretching ($\omega_x \partial u / \partial x$); (a-d) are at an intermediate time during vortex formation ($t^+ = 51$). The bold line in each panel identifies the ω_x layer.

5. Concluding remarks

To summarize, we have shown that nonlinearly evolving $w(x)$ disturbances of ejected low-speed streaks, initially without any vortices whatsoever, directly generates new streamwise vortices near the wall. The resulting 3D vortex geometry is identical to that of the dominant CS, deduced from fully developed near-wall turbulence, which in turn capture all important, extensively reported near-wall events. This serves as strong evidence that vortex-less streaks are the main breeding ground for new streamwise vortices, commonly accepted as dominant in turbulence production. In turn, the geometry of the newly generated vortices constitutes a built-in mechanism which sustains ejected streaks against their otherwise rapid self-annihilation due to cross-diffusion

of ω_y . Vortex-less streaks, the vehicle for vortex formation, are expected to arise inherently due to the differential advection of vortices and the streaks they generate.

Acknowledgements

This research was supported by AFOSR grant F49620-97-1-0131 and the NASA Graduate Fellowship grant NGT-51022 of W.S. Supercomputer time was provided by the NASA Ames Research Center.

References

- [1] Butler, K.M. & Farrell, B.F. 1992 Three-dimensional optimal perturbations in viscous shear flow. *Phys Fluids A* **4**, 1637.
- [2] Hamilton, J., Kim, J. & Waleffe, F. 1995 Regeneration mechanisms of near-wall turbulence structures. *J. Fluid Mech.* **287**, 317.
- [3] Hussain, F. 1986 Coherent structures and turbulence. *J. Fluid Mech.* **173**, 303.
- [4] Jeong, J. & Hussain, F. 1992 Coherent structures near the wall in a turbulent channel flow. In *Proc. of Fifth Asian Congress of Fluid Mech.*, Taejon, Korea (eds. K.S. Chang & H. Choi), p. 1262.
- [5] Jeong, J. & Hussain, F. 1995 On the identification of a vortex. *J. Fluid Mech.* **285**, 69.
- [6] Jeong, J., Hussain, F., Schoppa, W. & Kim, J. 1997 Coherent structures near the wall in a turbulent channel flow. *J. Fluid Mech.* **332**, 185.
- [7] Jimenez, J. & Moin, P. 1991 The minimal flow unit in near-wall turbulence. *J. Fluid Mech.* **225**, 213.
- [8] Jimenez, J. & Orlandi, P. 1993 The rollup of a vortex layer near a wall. *J. Fluid Mech.* **248**, 297.
- [9] Kim, J., Moin, P. & Moser, R.D. 1987 Turbulence statistics in fully developed channel flow at low Reynolds number. *J. Fluid Mech.* **177**, 133.
- [10] Kline, S.J., Reynolds, W.C., Schraub, F.A. & Rundstadler, P.W. 1967 The structure of turbulent boundary layers. *J. Fluid Mech.* **30**, 741.
- [11] Robinson, S.K. 1991 Coherent motions in the turbulent boundary layer. *Ann. Rev. Fluid Mech.* **23**, 601.
- [12] Schoppa, W., Hussain, F. & Metcalfe, R.W. 1995 A new mechanism of small-scale transition in a plane mixing layer: core dynamics of spanwise vortices. *J. Fluid Mech.* **298**, 23.
- [13] Schoppa, W. & Hussain, F. 1997 Genesis and dynamics of coherent structures in near-wall turbulence. In *Self-sustaining Mechanisms of Wall Turbulence* (ed. R. Panton). Computational Mechanics Publications, p. 385.
- [14] Schoppa, W. & Hussain, F. 1998a Formation of near-wall streamwise vortices by streak instability. *AIAA Paper No. AIAA 98-3000*.
- [15] Schoppa, W. & Hussain, F. 1998b A large-scale control strategy for drag reduction in turbulent boundary layers. *Phys. Fluids* **10**, 1049.

[16]Swearingen, J.D. & Blackwelder, R.F. 1987 The growth and breakdown of streamwise vortices in the presence of a wall. *J. Fluid Mech.* **182**, 225.

[17]Trefethen, L.N., Trefethen, A.E., Reddy, S.C. & Driscoll, T.A. 1993 Hydrodynamic stability without eigenvalues. *Science* **261**, 578.

[18]Yu, X. & Liu, J.T.C. 1991 On the secondary instability in Gortler flow. *Phys. Fluids A* **3**, 1845.

